The Design and Characterization of Scintillator Hodoscopes for SLAC Experiment E160

A thesis submitted in partial fulfillment of the requirement
for the degree of Bachelor of Science with Honors in
Physics from the College of William and Mary in Virginia,

by

Daniel Leo Bowring

Accepted for _____
(Honors, High Honors or Highest Honors)

_____
Advisor: Dr. Keith Griffioen

_____
Dr. Todd Averett

_____
Professor Kim Whitley

Williamsburg, Virginia
May 2002

Abstract

J/ψ and $\psi\prime$ particles can be produced by photons incident on a nuclear target. Detection of the J/ψ and $\psi\prime$ muon decay products allows for the determination of the dependence of J/ψ and $\psi\prime$ photoproduction on the size of nuclear targets, which is the intent of SLAC experiment E160. Planes of scintillator hodoscopes will be used to detect these product muons. Several characteristics of the individual scintillator/photomultiplier tube pairs must be determined in order to optimize the detector. Many of the hodoscope "fingers" will have epoxied joints. The optical qualities of these joints were tested using ^{106}Ru β-emission and cosmic ray coincidence measurements. The mechanical quality of these joints was also tested in preparation for the shipping process. Finally, the data acquisition system was assembled and tested using a μ cosmic ray detector.

Acknowledgements

First and foremost, I would like to thank Dr. Keith Griffioen, my research advisor, for his seemingly endless patience and support. I would like to thank Bryan Moffit for his work with the DAQ system, without which this project would be much less interesting. For their help in the machine shop preparing the scintillator joint faces, as well as their advice, I would like to thank Mel Woods and John Bensel. Finally, I'd like to thank Andrew T. Lane, who was working on a similar project, for his contributions and brainstorm-power in the laboratory.

Contents

1 Introduction

Experiment E160 [1] at the Stanford Linear Accelerator (SLAC) will measure the dependence of J/ψ photoproduction on the number of nucleons A in various nuclear targets. Photons can undergo quantum fluctuations, producing a charm/anti-charm ($c\overline{c}$) quark pair. Momentum transfer between this meson and a nucleon can induce the formation of a J/ψ particle in a reaction denoted as [2]

$$\gamma + N \rightarrow J/\psi + N \tag{1}$$

Information concerning this photoproduction is vital in determining the role J/ψ suppression plays in the formation of a quark-gluon plasma, which in turn will provide information about the structure of the universe very shortly after the big bang.

In the experiment, J/ψ's are produced by sending a beam of photons through a metallic target. This is accomplished in several steps. First, electrons from the SLAC linac with energies between 10 and 50 GeV are focused onto a thin diamond crystal. The slowing electrons in the target produce photons through bremsstrahlung, or braking radiation. Radiated photons are eliptically polarized according to interactions between the incident electrons and the crystal lattice, depending on the angle between the lattice and the incident beam [3]. The resultant coherent photon beam is directed at the nuclear targets shown in Table 1. When the $c\overline{c}$ meson interacts with the target, J/ψ's are produced.

Target Material	A-Value (Nucleons)
Be	9
Al	27
Cu	63
Pb	207

Table 1: Target materials used in E160.

The J/ψ lifetime is only about 8×10^{-19}s [4], so it must be studied through the products of its decay, specifically a muon pair (μ^+, μ^-). These muons must be detected amidst a huge background of photo-produced hadrons. An Al_20_3 absorber can effectively filter out these hadrons, as well as photons and electrons, leaving only muons. this is because muons are minimum ionizing and do not radiate like electrons becuase they are 200 times heavier. The muons are momentum analyzed using a large diploe magnet [1].

The muons are detected by using three separate planes of hodoscopes, which are arrays of scintillators attached to photomultiplier tubes (PMTs). Each hodoscope consists of both vertically and horizontally oriented scintillator fingers arranged in planes. When charged particles (including muons) pass through a scintillator, the molecules of scintillating material emit light which is internally reflected down the length of the scintillator and registered by the PMT at an end. The passage of the particle through a hodoscope will generate a signal in both a horizontally- and a vertically-oriented scintillator, giving us an x- and a y-coordinate with which to pin-point position. Tracking the particle's position allows the calculation of its trajectory and thus its energy and momentum. By tracking the paths of the two muons, the momentum vector of the J/ψ can be reconstructed.

2 Research Overview

The goal of this honors research project was the design and characterization of these hodoscopes. There are several scintillator characteristics that must be optimized for the specifics of the experiment. Some scintillators used in the experiment must be altered to fit the new detector geometry by joining two previously-used pieces with a UV-hardening epoxy. The optical qualities of this joint must be evaluated in order to determine the machining process appropriate for hodoscope construction.

In addition to the optical qualities of these joints, the mechanical integrity had to be measured in order to insure that the joints would not come loose in shipping or in use during the experiment. This evaluation ultimately involved ^{106}Ru β-emission coincidence testing, as well as the implementation of a data acquisition system that allowed simultaneous recording of time and light amplitude information from multiple scintillators, as used in the actual experiment. A sub-goal of this project, then, was to aid in the construction of the data acquisition system, including assembling racks of logic modules and designing the testing scheme.

3 The Basics of Particle Detection

3.1 Properties of Scintillators and PMTs

One of the basic forms of particle detector is the combination of a scintillator and a photomultiplier tube (PMT). Organic scintillators, or scintillators with organic molecules deposited in them, are characterized by their fast decay times and were used in this experiment. A scintillator is typically composed of a base plastic in which primary and secondary "fluor" molecules have been deposited [5]. When a charged particle passes through the plastic, it excites the primary material which radiates in the ultraviolet as it de-excites. In order to match the frequency of this emitted light with the frequency to which the PMT is most sensetive, wavelength shifting dye molecules are also dissolved in the scintillator plastic. The UV light emitted by the active scintillating material excites the dye molecules, such as anthracene, which emit bluish light [6]. This visible light can travel freely within the transparent plastic, propagating down the material via total internal reflection until it reaches the photomultiplier tube. There, a current is generated which is proportional to the light detected, which in turn is proportional to the energy deposited by the particle in the scintillator material.

The velocity of light in scintillator plastic, which has an index of refraction of approximately 1.5, is $v = \frac{c}{1.5}$. In addition, the average path that light takes through a scintillator can be up to 50% longer than the straightest path, due to reflection off the sides of the material. That means that for a one meter scintillator, light takes about 7.5 ns to travel from one end to the other. Finally, typical PMTs take approximately 2 ns to convert light into an electric current. The delay for this simple event, then, takes approximately 9.5 nanoseconds. This is well within the requirements of time resolution, when events occur between ten and thirty nanoseconds apart [5]. In this experiment, Bicron-408 and other similar scintillators are used, the properties of which are given in Table 3.1.

Property	Value for BC-408
Light Output, % Anthracene	64
Rise Time, ns	0.9
Decay Time, ns	2.1
Pulse Width, FWHM, ns	~2.5
Light Attenuation Length, cm	210
Wavelength of Max. Emission, nm	425
No. of H Atoms per cm^3, ($\times 10^{22}$)	5.23
No. of C Atoms per cm^3, ($\times 10^{22}$)	4.74
Ratio H:C Atoms	1.104
No. of Electrons per cm^3, ($\times 10^{22}$)	3.37
Principal uses/applications	TOF counters, large area

Table 2: Bicron-408. [7]

Photomultiplier tubes rely on the photoelectric effect to convert light incident on a photocathode into electrons with energy

$$eV = W - \hbar\omega \tag{2}$$

in which W is the work function of the photocathode. The freed electrons are guided from the photocathode through a series of electrodes called dynodes, each with a lower potential than the next. The dynodes emit secondary electrons when struck by a primary electorn. Each electron is accelerated through a potential before it strikes the dynode. It then continues to the next dynode, along with an average of four secondary electrons [8, 6]. This process repeats for each dynode, multiplying the number of electrons by a factor of δ. If there are N dynode stages in the PMT, the overall gain is given by

$$G = \delta^N. \tag{3}$$

Ultimately, the PMT creates a measurable voltage from a few photoelectrons. This voltage can be used to quantify the amount of light initially emitted by the secondary scintillating material. The PMT is a fairly fast device, with a typical rise time of two nanoseconds [5]. Therefore, the scintillator-PMT combination is well suited to accurate time-of-flight measurements. A signal from muon cosmic-ray detection is shown in Figure 1.

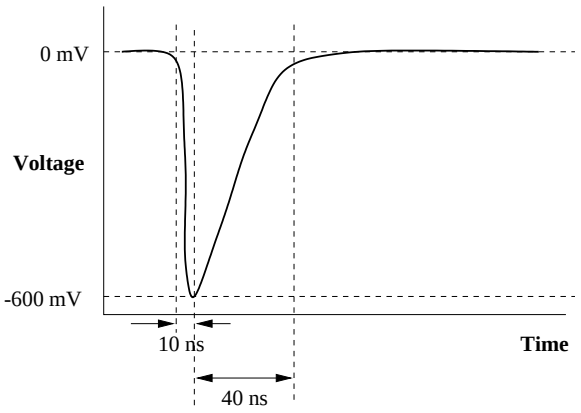

Figure 1: Schematic of voltage spike from PMT. This signal is typical of the 160 cm scintillators used for μ cosmic-ray coincidence measurements.

3.2 Particle Mass

The position and time-of-flight (TOF) measurements will chart each muon's path through the hodoscopes, yielding a 4-momentum $p_\mu = (E, \mathbf{p})$ for each detected muon. Here, E is the energy of the particle and $\mathbf{p}$ is its momentum vector. We can arrive at the mass of the J/ψ through simple energy considerations. If mass and momentum are written in units of energy,

$$(p_\mu)^2 = E^2 - \mathbf{p} \cdot \mathbf{p} = M_\mu^2 \tag{4}$$

where M_μ is the calculated mass of the detected muon. Recall that a J/ψ decays into a muon/anti-muon pair. The 4-momentum of the J/ψ, then, should be the sum of those of the two muons.

$$(E, \mathbf{p})_{J/\psi} = (E_{\mu^+} + E_{\mu^-}, \mathbf{p}_{\mu^+} + \mathbf{p}_{\mu^-}) \tag{5}$$

Using Equation 4, we can calculate the mass of the J/ψ ($M_{J/\psi}$) from the energy and momentum of its decay products.

$$(E_{\mu^+} + E_{\mu^-})^2 - (\mathbf{p}_{\mu^+} + \mathbf{p}_{\mu^-})^2 = {M_{J/\psi}}^2 \tag{6}$$

Here, $E_{\mu^\pm}$ and $\mathbf{p}_{\mu^\pm}$ are the energy value and momentum vector of the μ^+ and μ^- product particles.

4 Scintillator/PMT Characterization

Scintillators from hodoscopes used in SLAC experiment E155 will be used in the construction of hodoscopes for the current experiment. Although these recycled scintillators have the same cross-sectional area as those required for the new detector configuration, some of them must be joined to make longer pieces. The joint between these concatenated scintillators must be as optically transparent as possible to allow for efficient light transmission. To maximize transmission at the interface, the index

of refraction of the hardened adhesive must match that of the scintillator. Also, the machine used for preparing the joint faces must leave a smooth surface on the face of each piece. Any imperfections in the joint will result in imperfect light transmission across the joint, which translates to lost data. However, if the joint is too smooth, there will be a poor adhesive bond and the joint will be fragile. A goal of this project was to determine an effective balance betwen optical and mechanical joint quality.

4.1 Mechanical Methods of Joint Preparation

Three methods for preparing the faces of the joint were tested: an end mill facing, a fly cutter and a slitting saw.

End mills are tools commonly used in vertical milling machines and are similar to drill bits. The sides of an end mill are fluted, which means that when it spins it has two cutting surfaces. Bringing the tip to bear perpendicularly on a surface gives the end mill the function of a drill bit, making a circular hole in the material to be cut. The fluted side of the end mill can also be used to cut along the face of a material. It was this configuration that was used in preparing one of the scintillator joints. The side of the rotating end mill was drawn along the face of the scintillator, producing a flat surface.

A fly cutter is a single-point cutting tool similar to that used in a lathe. The base of the device houses the actual cutting point, which is a piece of tool steel set perpendicular to the axis of the mill. As the base rotates, the cutting point describes a circle of variable diameter. The entire device is mounted in a milling machine and brought into contact with the face of the material to be cut. As the material is fed past the fly cutter, the point of the device strips away very thin layers leaving a flat, smooth face.

Finally, the slitting saw is essentially a saw blade. Like the previous two cutting tools, the slitting saw is mounted in a milling machine. The saw functions much as

a circular saw, making deep, narrow grooves in the material to be cut. In this case, the slitting saw was drawn completely through the scintillator.

4.2 Preparation of the Test Scintillators

Each of the three jointed scintillators in the test set were prepared identically. A bandsaw was used to cut a length of 2.54 $\times$ 1.27 cm scintillator into three segments between 24 and 26 cm long. Note that, because light attenuates so little in the scintillator, the exact length of each test piece has little bearing on the final measurements. For polished Bicron-408, the 1/e attenuation length of light is 210 cm [7]. Over a length of 25 cm then, light travelling directly between its point of origin and the PMT will attenuate by a factor of only 4.38×10^{-2}. For test purposes, this factor is negligible. The faces of the scintillator pieces were then prepared using the three methods described in Section 4.1. After the joints were mechanically prepared, each face was polished by hand until transparent using Microgrit, a powder-based polish manufactured by the Micro Abrasives Corporation. The pieces were then joined using an Emerald Green Spot UV lamp with "Dymax ultra light-weld" UV light curing adhesive. The entire joined piece was then polished, wrapped in a layer of reflective Mylar and, after abutting an end to a photomultiplier tube, the whole assembly was covered with electrical tape. This process makes the scintillator opaque to external light, internally reflective and ready for particle detection.

Each jointed scintillator/phototube was then tested for light-tightness. The phototubes were connected to a voltage source and the outputs were monitored on an oscilloscope. Gaps in the electrical tape were then found by shining a flashlight along the scintillator and watching for a PMT signal on the oscilloscope, indicating light detection.

4.3 ^{106}Ru β-source Testing

The optical quality of the joint was first tested by measuring the coincidence of β-ray emission counts between two overlapping scintillators, one integral and one with a joint in the middle. A collimated ^{106}Ru β source was positioned at the intersection between both scintillators. In one arrangement, the coincidence is measured so that the propagating light in the jointed scintillator must pass through the joint. In the other, coincidence is measured between the joint and the PMT, so that the photons can travel between their origin and the PMT unhindered. Figure 2 is a simple diagram of this setup. In each configuration, β-decay count rates are measured. The greater

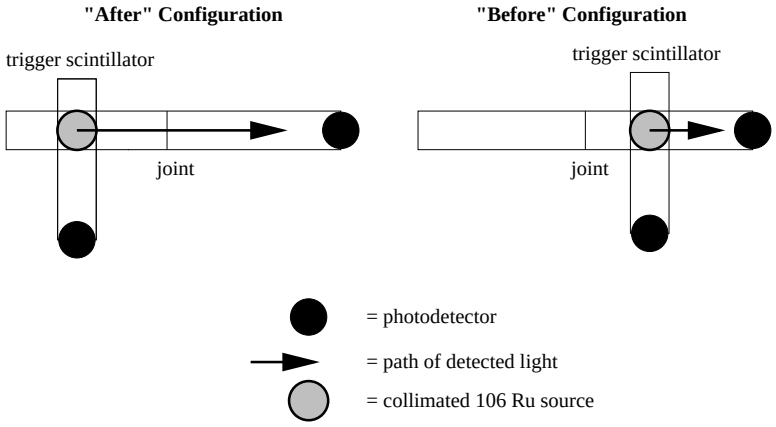

Figure 2: Diagram of two configurations for ^{106}Ru coincidence measurements.

the difference in measurements between configurations, the less transparent the joint must be. A set of measurements for each joint type is given in Section 9.1 in the Appendix.

It's clear from the data that this method of measurement is not very effective in determining joint quality. If the ratio of average count rates before and after the joint are analyzed, it seems as though the slitting saw provides the most transparent joint. That is, the data indicate that the highest fraction of signals are being transmitted through the slitting saw joint. However, the count rates before and after the joint for each joint type are very close together and in some cases they even overlap. Consider

the case of the end mill, where there seems to be a higher count rate when the signal must pass through the joint. This seems nonphysical in that the joint appears to be a more efficient signal transmitter than does the integral scintillator piece. These ambiguities in the data suggest that many measurements must be taken before reliable data can be obtained. Since coincidence measurements of 1% error using the ^{106}Ru β-source take anywhere between ten and fifty minutes each, it appears that a faster method of measurement must be used for accurate analysis. A definitive analysis of these qualities would require many more data points than are shown here and the time needed for these measurements becomes very long. As an alternative, the data acquisition system (DAQ) was used. This system, designed for data collection in E160, allows for the rapid collection of large amounts of data, which appears to be necessary for the accurate evaluation of joint quality.

5 The William and Mary DAQ System

The William and Mary data acquisition system (DAQ) was developed by graduate student Bryan Moffit as a tool for taking fast, automated measurements of particles incident on the detectors. Currently, "fast" means up to 1000 events per second. This is well within the parameters for muon cosmic-ray flux, the count rates for which are approximately 100 per second in the test detector. The output of each photomultiplier tube is routed through a system of electronics which converts the signal from a raw voltage spike to a signal that can be interpreted by the DAQ modules. That signal is sent to a time-to-digital converter (TDC), a charge-to-digital converter (QDC) and a scaler. These logic modules communicate via VME with the data acquisition program, which can determine the charge of an incident particle and/or where this particle passed through the detector. The flexibility of this system makes it useful for many detector configurations.

The entire data acquisition system can be separated into three distinct parts: the detector itself, the electronics associated in converting the raw detector signal into something interpretable by a computer, and the data acquisition software. The VME-based modules that communicate with the DAQ software have thirty-two available channels for signal input, so a wide range of detectors may be used.

5.1 The Muon Cosmic-Ray Detector

Elements of the third hodoscope plane for E160 were assembled into a simple muon cosmic-ray detector and tested using the William and Mary DAQ. The detector is composed of two 160 $\times$ 10 $\times$ 10 cm scintillators, one on top of the other, both with photomultiplier tubes at each end. When a cosmic ray passes through the detector, it is possible to reconstruct its trajectory based on the firing times and signal amplitudes of the four PMTs. The fact that two scintillators are used minimizes the contribution of random noise, as the detector's logic modules (see Section 5.2) eliminate potential events that are not registered by all four PMTs. To ensure the exclusive detection of cosmic-ray muons, the detector is housed in a darkroom. This eliminates the possibility of any light entering the scintillators and being mistaken for an event. When a muon cosmic ray passes through the detector, it generates light within the scintillators which is converted into a voltage spike by the photomultiplier tubes, as described in Section 3.1. This current is passed to an array of logic modules designed to prepare that raw voltage spike for the DAQ software (see Section 5.2).

5.2 Logical Signal Processing

The goal of the system of logic modules is to convert the signals generated by the PMTs into data which is readable by the data acquisition system. There are three VME-based C.A.E.N. modules used in the DAQ for which the array of logic modules must prepare the signal: the time-to-digital converter (TDC), the charge-to-digital

converter (QDC) and the scaler.

5.2.1 Charge-to-Digital Conversion

The C.A.E.N. model V792 32-channel QDC module measures the total amount of charge which passes through each channel during a given time interval. Recall that the PMT sends as its output a raw voltage spike, depicted in Figure 1. When it receives the falling edge of a negative NIM logic pulse in the Common Start (COM) port, the device begins charging a capacitor with the input current from the PMT. This happens for each channel of input. The discharge time of this capacitor is measured by counting the periods of a high-frequency signal which cycles between the rise and fall of a trigger signal. The QDC then integrates over the charge time of the capacitor to determine the total charge stored in the capacitor. This value is then sent to the DAQ software as the total charge seen by the QDC, which is proportional to the amount of energy deposited in the scintillator by the incident particle.

5.2.2 Time-to-Digital Conversion

The C.A.E.N. model V775 32-channel TDC functions in much the same was as the QDC. Between the rise and fall of a trigger signal, the unit charges a capacitor with a metered current. The unit then measures the discharge time of the capacitor by counting high-frequency clock pulses. This yields a high-resolution time value for the response of each PMT using the first detected signal to start the clock. These digitised times are likewise fed to the DAQ software.

5.2.3 Scaler

The C.A.E.N. mdoel V560N 16-channel scaler simply increments a counter for each logic pulse sent to the COM port. This information is sent to the DAQ software in order to construct a list of events and their associated time and charge information.

5.2.4 Signal Conversion Via Logic Modules

In light of the signal requirements of the QDC, TDC and scaler as described above, the original PMT signals must be modified. Each signal has a fairly sharp rise time but a comparatively long decay time, making it difficult to pinpoint when each signal ends. In order to convert these raw signals into something readable by the TDC, QDC and scaler, additional logic modules must be used.

The initial signals are first sent to a LeCroy model 428F linear fan-out module, which duplicates the signals. The fan out generates four output signals identical to each input signal it receives. In this case, the fan-out produces a pair of identical signals from each PMT. The first set of signals is sent through delay cable to the QDC. Note that the modules use a NIM-format signal, which is a standard developed in the 1960s to promote the compatability of devices [9]. For example, NIM fast-negative logic standards require true and false voltage levels to correspond to -0.8V and 0V respectively [9]. The QDC, on the other hand, requires an emitter-coupled logic (ECL) pulse. Proper equipment was not available to make this conversion cleanly, so a kludge was used: the NIM pulses were sent through BNC cables which terminated in bare wires for negative and ground. These wires were then attached to the inputs of the ribbon cable leading to the QDC input. Although this solution leaves impedences mismatched between the cables used for the NIM units and the BNC kludge cables (50 ohms vs. $\sim$200 ohms), it provides a signal which is of sufficient quality for testing purposes. The other set of signals from the fan-out is sent through a series of logic modules that, in addition to generating this COM logic pulse, convert the signals into logic pulses readable by the TDC and scaler.

The second set of signals from the fan-out are sent to a Phillips Scientific model 711 six-channel discriminator, which converts the PMT voltage spikes into logic pulses. Each PMT signal now has a definitive beginning and end, established by setting a threshold value on the discriminator module. The four logic pulses are fanned out of

two output channels each, to be used for two different operations.

The first set of signals is sent through delay lines to a LeCroy model 4616 ECL-NIM-ECL module, which converts the NIM signals used in the other modules into an ECL pulse required by the TDC. Delay lines are used so that the signals themselves arrive after the trigger. The second set is sent to a LeCroy model 4616 coincidence unit to create that trigger. This module performs a simple logical AND operation. If the pulses from the four PMTs occur within a specified window of time, they are deemed to be resultant from a single particle passing completely through both scintillators. The AND operation combines these four pulses into a single logic pulse with a leading edge corresponding to that of the first PMT signal in time and a falling edge corresponding to the fall of the last PMT signal. This OR pulse is sent through another discriminator to the TDC, QDC and scaler in order to start the timing mechanisms in the former devices and to increment the event count in the latter. Figure 3 is a simplified schematic of this process.

5.3 DAQ Software

The DAQ software connects with the TDC, QDC and scaler via telnet and collects time and light amplitude data for each detected event. At the end of a user-specified number of counts, the software generates a data file containing this information for each event. A fortran program (see Appendix 9.2) gathers this data into a type of array called an "ntuple" in Physics Analysis Workstation (PAW). Histogram plots of ntuple data for each channel of information are shown in Appendix 9.3. PAW can then be used to analyze these values.

The resolution of the detector can be determined by calculating the particle position in the detector two ways and examining the linearity between them. For a scintillator of length L, the TDC value from the PMT at either end can be used to determine the position of the incident particle. The TDC measures a time for the

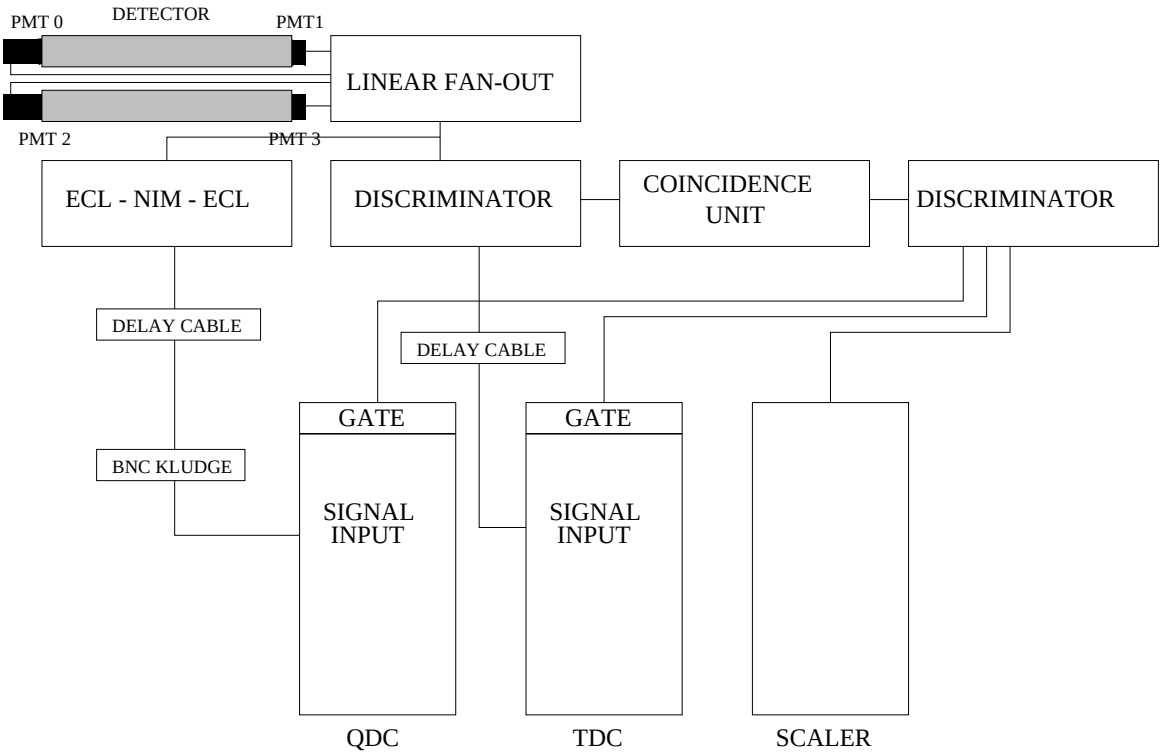

Figure 3: Simple schematic of logic modules.

first PMT

$$T_1 \;=\; t_0 \;+\; \frac{x}{v} \tag{7}$$

where t_0 is the time between the actual PMT detection of the signal and the arrival of that signal at the TDC, x is the distance from the end of the scintillator and v is the speed of light within the scintillator. The PMT at the other end of the scintillator will give a slightly different TDC value. In this case,

$$T_2 \;=\; t_0 \;+\; \frac{L-x}{v} \tag{8}$$

Normally, the TDC gives time values that are heavily scaled. When considering the TDC time values, one must consider each step in the path of the signal which takes a non-negligible amount of time, adding to the value of t_0. Without considerable efforts at calibration, single TDC values are relatively meaningless. However, the difference between the two TDC values for each scintillator (Δt) subtracts out the offset, leaving

us with sensible values.

$$\Delta t \;=\; T_1 - T_2 = \frac{2x - L}{v} \tag{9}$$

Solving for x, the position of the detected particle, we get

$$x = \frac{v}{2}\Delta t + \frac{L}{2} \tag{10}$$

Another way to arrive at a value for x is through QDC data. Assuming that the intensity of light decays exponentially with the distance it travels in a scintillator, we can write

$$A = A_0 e^{-\frac{x}{\alpha}} \tag{11}$$

where A_0 is the initial intensity of the light generated, A is the light intensity at the phototube, x is the distance between the point of generation and the PMT, and α is the attenuation length of the scintillator. In the case of Bicron-408 scintillator material, $\alpha = 210$ cm (see Table 3.1). QDC values are scaled throughout the DAQ system. That is, the PMT voltage is proportional to the light detected, which in turn is proportional to the energy deposited in the scintillator, etc. Since it would be difficult to determine A_0 without significant calibration, the ratio of two amplitudes are compared. This allows for a calculation of x without having to consider A_0 at all. Let the intensity of light at each phototube on a scintillator be written as $A_1 \;=\; A_0 e^{-\frac{x}{\alpha}}$ and $A_2 \;=\; A_0 e^{-\frac{(L-x)}{\alpha}}$. Then,

$$\frac{A_1}{A_2} = e^{-\frac{(2x-L)}{\alpha}} \tag{12}$$

Solving for x, we get

$$x = \frac{\alpha}{2}\ln\left(\frac{A_1}{A_2}\right) + \frac{L}{2} \tag{13}$$

Since Equations 10 and 13 represent the same value of x, plotting them against each other should yield a straight line. The spread of data points on a scatter plot of x_{TDC} vs. x_{QDC} indicates the efficiency of the detector.

For the μ cosmic-ray coincidence detector, we can follow the above equations. $L = 160$ cm and $\alpha = 210$ cm. When we plot Eq. 10 against Eq. 13 for both detector

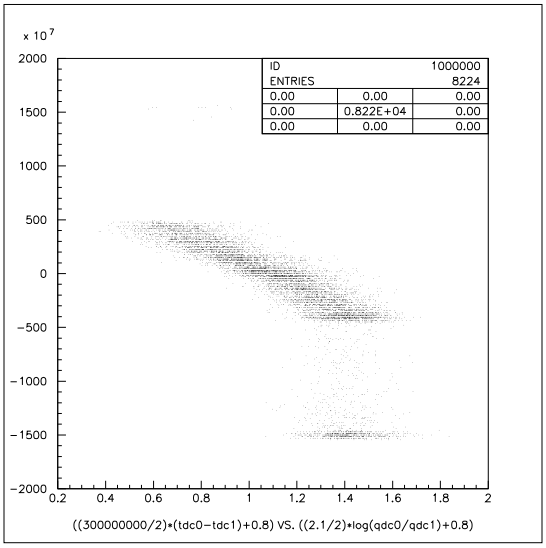

Figure 4: Particle position x in the first scintillator derived from TDC data vs. x derived from QDC data.

scintillators, we get Figures 4 and 5. For the most part, these graphs are linear. The cluster of points towards the bottom of Figure 4 can be attributed to faulty equipment. Specifically, one of the PMTs in the first scintillator consistently generated a signal with a lower amplitude than the other PMTs. The background noise could then interfere more with the calculation of the signal width, skewing some TDC data. This could explain why the TDC data appears unusually low, while the QDC values follow the trend.

6 Methods of Mechanical Characterization

In addition to the optical quality of the joint, the mechanical quality must also be considered. Once the hodoscopes are constructed, they will be shipped to Stanford, CA in crates. If the detector is damaged during that process, there will be considerable delays while it is shipped back to Williamsburg for repairs. It is convenient to know

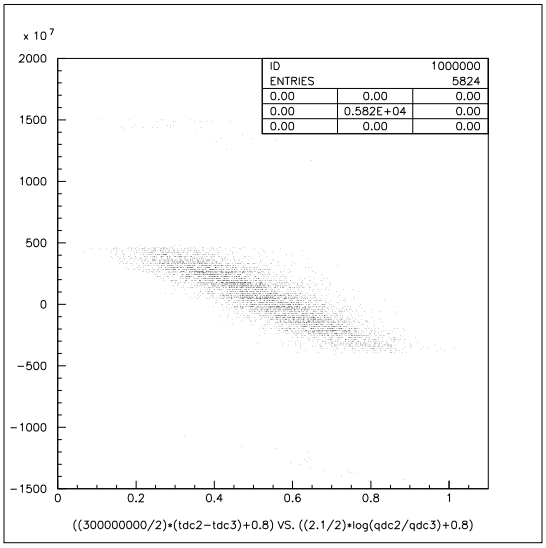

Figure 5: Particle position x in the second scintillator derived from TDC data vs. x derived from QDC data.

the mechanical strength of the joints ahead of time so that necessary precautions can be taken during the construction of the actual hodoscopes. There is a tradeoff here between the optical and mechanical quality of the joint. Obviously, smoother surfaces at the joint will be more transparent and will register more of the incident particles more accurately. The smoother these surfaces become, however, the more tenuous the adhesive bond between them will be. The strength of the joint was measured by suspending a weight from the end of a scintillator and noting the largest torque it could withstand before the material degraded via stress fractures, bending, complete breakage, etc. The actual setup used for this part of the experiment is illustrated in Figure 6.

Three parameters were measured in the evaluation of the mechanical quality of the joints: torque applied for crazing (stress cracks) of the plastic, bowing of the scintillator when crazed, and torque applied before complete mechanical failure. The results are shown in Table 6. The data for the end mill joint are not available.

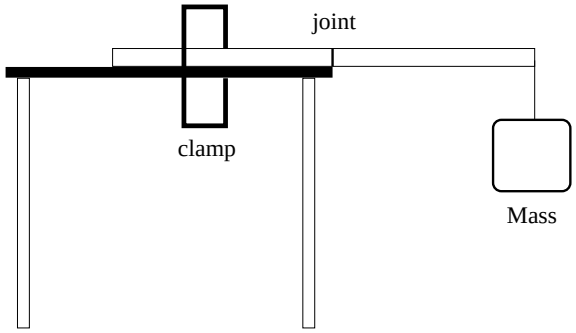

Figure 6: Method of testing mechanical quality of epoxy joint.

Joint Type	Torque At Crazing (Nm)	Bowing (Radians)	Torque At Breaking (Nm)
Fly Cutter	0.49	0.03	1.47
Slitting Saw	0.49	0.02	1.67
End Mill	N/A	N/A	N/A

Table 3: Parameters of mechanical joint quality. Note that crazing occurred only on the face of the scintillators, leaving the centers relatively clear.

This piece broke at the joint when it was being clamped to the lab table. A possible explanation for this is that the two pieces of the scintillator were not alligned properly during the original gluing. When a shim, used to keep the clamp from pressing directly on the scintillator, pressed against the joint, the unevenness caused enough stress to damage the piece. As this did not happen with the other, similarly prepared joints, it is safe to assume that the end mill joint was the weakest. The joint from the slitting saw proved to be strongest, since it withstood the most torque before breaking.

7 Conclusions

One of the goals of this research project was to evaluate the mechanical and optical qualities of the three different joint types. It is evident from the data that the slitting saw provided the best of both worlds. Not only did it transmit the most light during

coincidence testing, but it withstood the most torque before breaking as well. From the data available, the slitting saw appears to provide the best joint face between scintillators. However, more measurements must be made before this can be affirmed as fact. There was not enough time to perform μ cosmic-ray coincidence on the three different joint types using the DAQ system, so analysis must be made on the exisiting, small data set. Also, due to limited materials, only one trial of mechanical joint strength could be made for each joint type. Conclusions as to the absolute mechanical strength of a joint must be made after many more trials.

As for the μ cosmic-ray coincidence detection system in general, it is evident from the data in Table 9.1 that more trials are needed. Consider the data for the end mill joint coincidence, wherein the joint is a better transmitter of light than plain, integral scintillator. Taking more data will allow us to determine whether the source of this discrepancy. Although more research is needed, the fact that Figures 4 and 5 approach linear suggests that the methods of joint preparation are viable. Consider that all three scintillator joints were prepared by hand. The system was still capable of producing results that, while not perfect, are sensible enough to draw conclusions from. By improving the mechanical techniques involved in joining scintillators, such as standardizing the UV adhesive procedure, the data can be made even more sensible. With further research and improvements, the current procedure could yield high-quality scintillators usable in experiment E160.

8 In The Future

Old hodoscopes from SLAC E155 are available for testing. The most complex detector setup to date has only required the data acquisition system to handle four channels of information simultaneously. In order to refine the system, the DAQ can be used to test these old hodoscopes. That way, there will be conclusive evidence that the system

is capable of handling many channels of information and very high count rates. In addition, techniques must be developed for mass-producing the scintillators required for the assembly of the final detector. Although the final shape of the detector is as yet undetermined at the time of writing, it will ultimately need approximately five hundred of these jointed scintillators, each of specific lengths.

References

[1] V. Ghazikhanian, *et al.* "Proposal to Measure the A-Dependence of J/ψ and $\psi\prime$ Photoproduction," 2000. Available at: $http://www.slac.stanford.edu/exp/e160/jpsi.pdf$

[2] J. M. Laget, "The photoproduction of vector mesons," Nucl. Phys. A **699**, 184 (2002) [arXiv:hep-ph/0107208].

[3] D.R. Walz. "Polarized Photon Source: Coherent Bremsstrahlung Beams From Single Crystal Diamond Targets For E-159, E-160 & E-161," March 29, 2001. Available at: $http://www.slac.stanford.edu/exp/e159/doe01DWa.pdf$

[4] R. Nave. "Hyper Physics," 2000. Available at: $http://hyperhpysics.phy-astr.gsu.edu/hbase/particles/hadron.html\#c5$

[5] D. Green. "The Physics of Particle Detectors," (Cambridge University Press, New York, 2000.)

[6] D.H. Perkins. "Introduction to High Energy Physics," (Addison-Wesley Publishing Company, Inc., New York, 1987.)

[7] Bicron company website. $http://www.bicron.com/bc408.htm$

[8] I.R. Kenyon. "Elementary Particle Physics," Routledge & Kegan Paul, 1987. New York.

[9] "An Introduction to NIM". Available at the Fermilab PREP Equipment Pool's Electronic Equipment Information page: $http://www-esd.fnal.gov/esd/catalog/intro/intronim.htm$

[10] H. Frauenfelder, E.M. Henley. "Nuclear and Particle Physics," (W.A. Benjamin, Inc., Reading, 1975.)

[11] D.E. Groom, *et al.* "Cosmic Rays," February 2000. p. 4. Available at: *http* : *//pdg.lbl.gov/*2001/*cosmicraypp.pdf*

[12] G.F. Knoll. "Radiation Detection and Measurement," (John Wiley & Sons, New York, 2000.)

[13] W.R. Leo. "Techniques for Nuclear and particle Physics Experiments: a How-To Approach," (Springer, New York, 1994.)

9 Appendix

9.1 Coincidence Measurement Data

Joint Type	N/t "Before"	N/t "After"	Ratio of Average $\frac{\text{"}After\text{"}}{\text{"}Before\text{"}}$ Count Rates
Slitting Saw	16.1314	7.2389	
	11.6835	9.3503	
	12.2036	11.4426	
	12.9529	5.5381	
	10.2090	9.6308	
	15.8321	12.6995	
	15.7823	12.5232	
	15.5072	12.4445	
Average Val.	13.7878	10.1085	0.7331
Fly Cutter	7.8026	10.2987	
	7.8300	9.8447	
	7.4621	6.7856	
	10.7102	8.3768	
	10.7267	7.7450	
	10.5412	4.4026	
	10.4080	4.6883	
	10.5724	3.3574	
Average Val.	9.5157	6.9374	0.7290
End Mill	11.0452	15.9365	
	11.3737	11.5114	
	11.5626	10.3502	
	11.7438	10.1139	
	11.4811	16.5565	
	11.5350	16.9848	
	10.2647	17.2489	
	10.3054	17.5529	
Average Val.	11.1594	14.5319	1.3022

Table 4: Typical count rates for different scintillator joints. "After" denotes the configuration in which signals must pass through the joint. "Before" denotes the configuration in which signals may pass unimpeded to the phototube. Please note that the "before" and "after" values are placed side-by-side for convenience and not because of any relation between two specific values. N/t denotes counts per second.

9.2 bigdaq.kumac

The following program is a kumac written to convert a DAQ-generated data file (one event per line) into an ntuple that can be processed by Physics Analysis Workstation.

```
MACRO BIGDAQ


Ntuple/create 100 'W&M Physics DAQ' 29 ' ' ! _
Event adc_0 adc_1 adc_2 adc_3 adc_4 adc_5 adc_6 adc_7 adc_ev _
tdc_0 tdc_1 tdc_2 tdc_3 tdc_4 tdc_5 tdc_6 tdc_7 tdc_ev _
scaler_0 scaler_1 scaler_2 scaler_3 scaler_4 scaler_5 scaler_6 scaler_7 _
FSR Iped
Ntuple/read 100 bigrun
Histo/file 1 bigrun.hbook 1024 N
hrout 100
ntuple/print 100
zone 1 2
opt stat
set stat 110
set htyp 244
Ntuple/plot 100.adc_6
Ntuple/plot 100.adc_7
Close 1
zone
hi/de 100
RETURN
```

9.3 DAQ Histograms

The following figures are histograms of typical DAQ data. 10,000 events of μ cosmic-ray coincidences are binned according to the unscaled TDC and QDC values recorded by the DAQ.

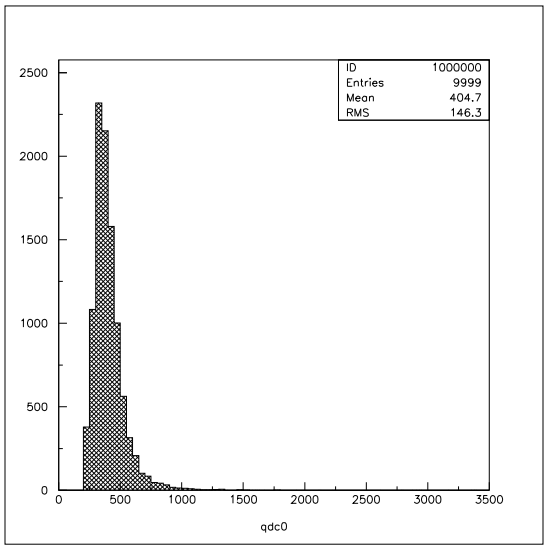

Figure 7: Histogram of events for the 0^{th} QDC channel for μ cosmic-ray coincidence.

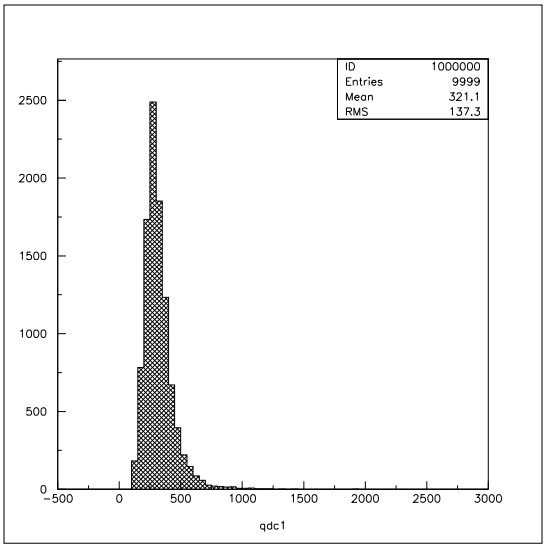

Figure 8: Histogram of events for the 1^{st} QDC channel.

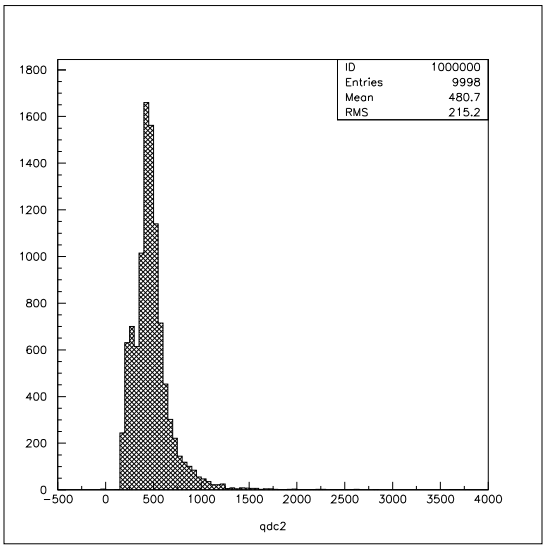

Figure 9: Histogram of events for the 2^{nd} QDC channel.

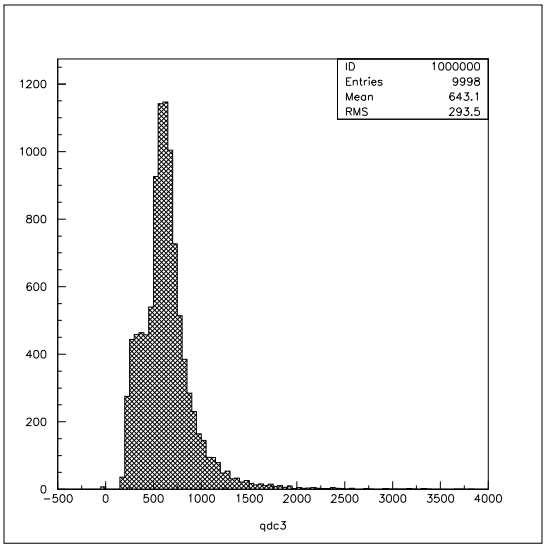

Figure 10: Histogram of events for the 3^{rd} QDC channel.

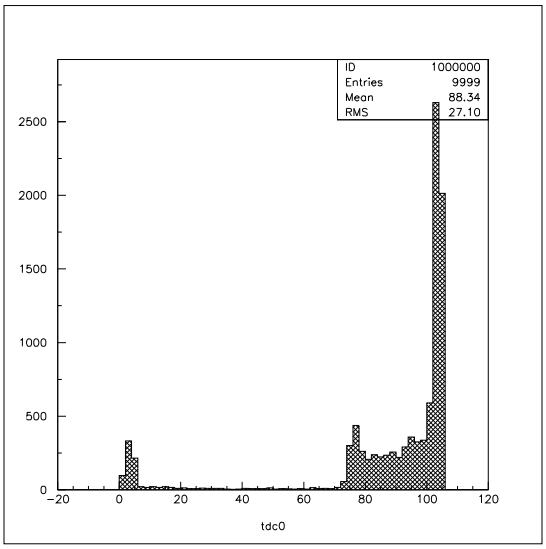

Figure 11: Histogram of events for the 0^{th} TDC channel for μ cosmic-ray coincidence.

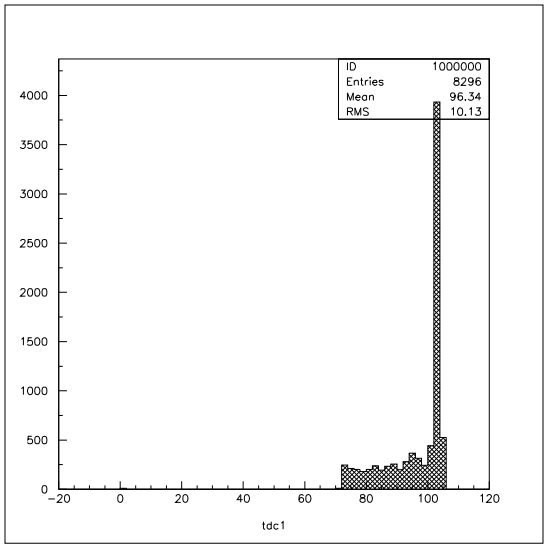

Figure 12: Histogram of events for the 1^{st} TDC channel.

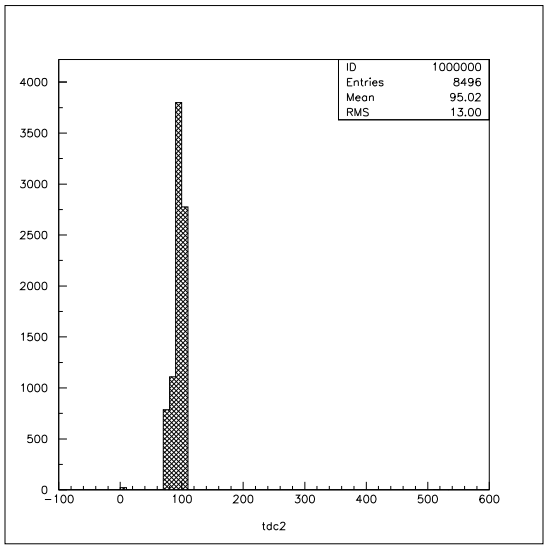

Figure 13: Histogram of events for the 2^{nd} TDC channel.

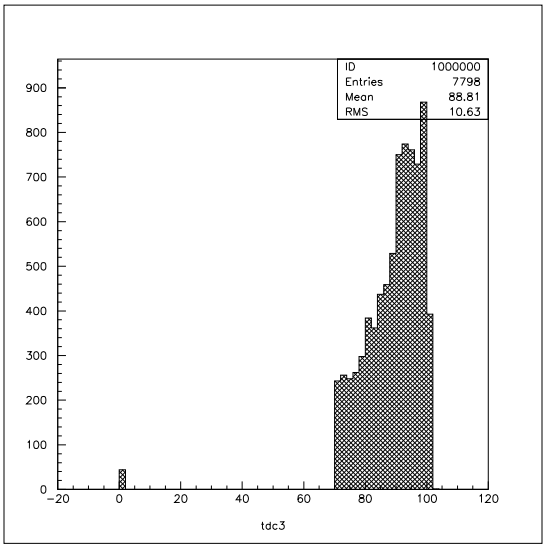

Figure 14: Histogram of events for the 3^{rd} TDC channel.